Received: 8 May 2022 | Revised: 13 October 2022 | Accepted: 18 October 2022

DOI: 10.1002/esp.5515

RESEARCH ARTICLE

ESPL WILEY

A hydraulic modelling approach to study flood sediment deposition in floodplain lakes

Joeri B. Reinders[1] | Richard M. Sullivan[2] | Tyler S. Winkler[2,3] | Peter J. van Hengstum[2,4] | R. Edward Beighley[5] | Samuel E. Munoz[5,6]

[1]Leiden University College, Leiden University, The Hague, the Netherlands

[2]Department of Oceanography, Texas A&M University, College Station, Texas, USA

[3]Department of Geology and Geophysics, Woods Hole Oceanographic Institution, Woods Hole, Massachusetts, USA

[4]Department of Marine and Coastal Environmental Science, Texas A&M University at Galveston, Galveston, Texas, USA

[5]Department of Civil and Environmental Engineering, Northeastern University, Boston, Massachusetts, USA

[6]Department of Marine and Environmental Sciences, Marine Science Center, Northeastern University, Nahant, Massachusetts, USA

Correspondence
Joeri B. Reinders, Leiden University College, Leiden University, The Hague, 2595DG, the Netherlands.
Email: j.b.reinders@luc.leidenuniv.nl

Funding information
US National Science Foundation, Grant/Award Numbers: EAR1804107, EAR-1833200

Abstract

Abandoned river channels on alluvial floodplains represent areas where sediments, organic matter, and pollutants preferentially accumulate during overbank flooding. Theoretical models describing sedimentation in floodplain lakes recognize the different stages in their evolution, where the threshold for hydrological connectivity increases in older lakes as a plug-bar develops. Sedimentary archives collected from floodplain lakes are widely used to reconstruct ecological and hydrological dynamics in riverine settings, but how floodplain lake evolution influences flow velocities and sedimentation patterns on an event scale remains poorly understood. Here we combine sediment samples collected in and around a floodplain lake with hydraulic modelling simulations to examine inundation, flow velocity, and sedimentation patterns in a floodplain lake along the Trinity River at Liberty, Texas. We focus our analyses on an extreme flood event associated with the landfall of Hurricane Harvey in August 2017 and develop a series of alternative lake bathymetries to examine the influence of floodplain lake evolution on flow velocity patterns during the flood. We find that sediments deposited in the lake after the Hurricane Harvey flood become thinner and finer with distance from the tie-channel in accordance with simulated flow velocities that drop with distance from the tie-channel. Flow velocity simulations from model runs with alternative plug-bar geometries and lake depths imply that sedimentation patterns will shift as the lake evolves and infills. The integration of sediment sampling and hydraulic model simulations provides a method to understand the processes that govern sedimentation in floodplain lakes during flood events that will improve interpretations of individual events in sedimentary archives from these contexts.

KEYWORDS
flooding, floodplain lakes, hurricane Harvey, hydraulic modelling, sediment transport

1 | INTRODUCTION

Alluvial floodplains constitute a major store of material transported by rivers including sediments, organic material, and pollutants (Asselman & Middelkoop, 1995; Ciszewski & Grygar, 2016; Phillips et al., 2004; Thoms, 2003; Walling & Bradley, 1989). Abandoned channels—floodplain depressions that form as a result of avulsion, meander cutoffs, or lateral channel migration—are particularly efficient sediment traps due to their geometry and proximity to the active river channel (Gilli et al., 2012; Munoz et al., 2015; Rowland et al., 2005; Toonen et al., 2012). Theoretical models describing the long-term evolution and infilling of abandoned channels generally recognize two major phases: a transitional phase and the abandoned phase (Gagliano & Howard, 1984; Toonen et al., 2012). The transitional phase follows lake formation and is marked by regular inundation of the lake (Gagliano & Howard, 1984; Toonen et al., 2012).

Sediments deposited in the lake during the transitional phase are typically coarse-grained sands deposited in thick sequences, and result in the formation of a plug-bar at the lake entrance, and narrowing and shallowing of the lake arms (Douglas Shields & Abt, 1989; Toonen et al., 2012). As a mature plug-bar develops, the lake floods less frequently and moves towards the abandoned phase (Amoros & Bornette, 2002; Hudson et al., 2012). Sedimentation during the abandoned phase is recognized as laminated fill, in which coarse-grained bedload accumulates in the lake during infrequent overbank flooding while finer-grained autochthonous material is deposited during non-flood conditions (Toonen et al., 2012, 2015). The process of infilling continues to decrease water depth in the lake until the abandoned channel is completely filled with sediment (Gagliano & Howard, 1984).

Controls on the overall rate, distribution, and characteristics of floodplain lake infilling are contingent on the sediment load of the main channel, the trapping efficiency of the lake, and the hydrological connectivity of the lake (Citterio & Piégay, 2009; Cooper & McHenry, 1989). Sediment concentrations in the river are mediated by watershed scale processes, such as the geology, land use, and basin climatology. Individual lake hydrological connectivity and trapping efficiency (i.e., the ability of the lake to retain sediments) depend on local geomorphic conditions and change over time as the lake evolves and infills (Citterio & Piégay, 2009; Douglas Shields & Abt, 1989). Trapping efficiency is controlled by lake geometry (Citterio & Piégay, 2009; Constantine et al., 2010)—for example, the shape, channel slope, depth, and diversion angle from the river (Douglas Shields & Abt, 1989; Fisk, 1948). Hydrological connectivity represents the synchronicity between stage levels in the river and lake (Hudson et al., 2012), and depends on the magnitude and frequency of flooding on the river, and topographic features in and around the lake (Amoros & Bornette, 2002). Plug-bar and tie-channel morphology are particularly important in the transfer of water and sediment between the river and lake (Hudson et al., 2012; Rowland et al., 2005), partly because the increased elevation of the plug-bar over time increases the threshold for hydrological connectivity (Hudson et al., 2012). As such, younger floodplain lakes frequently receive water and sediment through tie-channels whereas older lakes become increasingly isolated from the main channel (Citterio & Piégay, 2009; Hudson et al., 2012).

Theoretical models and observations provide valuable parameters to understand long-term sediment accumulation in floodplain lakes, but they are less well suited to explain the event-to-event variation in flood deposits within sedimentary archives. Sedimentary archives from floodplain lakes are widely used to reconstruct ecological (Bartlein et al., 2011; Bhattacharya et al., 2016; Brugam & Munoz, 2018; Liu et al., 2012; McGlue et al., 2016; Munoz et al., 2014; 2019) and hydrological (Leigh, 2018; Munoz et al., 2015, 2018; Toonen et al., 2015, 2020) dynamics in riverine environments. In these latter applications, laminated sequences are interpreted in terms of sedimentation during floods, where coarse-grained event beds are used as proxies for flood occurrence (Munoz et al., 2015; Toonen et al., 2016) and magnitude (Toonen, 2015), and finer-grained material deposited during non-flood conditions can, for example, preserve geochemical and biological proxies (Bhattacharya et al., 2016). The interpretation of these sedimentary archives relies on geomorphic stability of the floodplain and river—a condition that is challenging to meet given the dynamic nature of alluvial systems (Dee et al., 2018; Lecce et al., 2004).

The long-term process of floodplain lake evolution is likely to progressively affect patterns of sediment accumulation through its influence on hydrological connectivity and lake bathymetry, making individual event layers in sediment archives highly time and context dependent. Hydraulic models could offer an opportunity to better understand the processes that mediate sediment accumulation in floodplain lakes during floods without having to rely on extensive data collection. Here, we combine field-based sampling and observations of sediments in and around a floodplain lake with hydraulic modelling to examine patterns of sedimentation, flow velocity, and inundation extent in the context of an extreme flood. We focus our analysis on a floodplain lake of the Trinity River (Texas) and the recent extreme flooding associated with the landfall of Hurricane Harvey in August of 2017 (Blake & Zelinsky, 2018). We construct a hydraulic model using HEC-RAS (Hydrologic Engineering Center—River Analysis System), a publicly available modelling platform developed by the US Army Corps of Engineers that is commonly used in flood inundation mapping (Brunner, 2021a). We use grain-size analysis of sediment samples from point-bars, a tie-channel, and the lake-bottom to document how sediments are mobilized and deposited during an extreme flood, while hydraulic simulations of the same event provide insights into the flow velocities that give rise to these sedimentation patterns. We then use our hydraulic model to evaluate how floodplain lake evolution influences patterns of flow velocity by developing a series of alternative lake bathymetries where the plug-bar and lake depth are varied. These analyses demonstrate that the properties of the sediment layer deposited by a certain flood magnitude change as floodplain lake geometry and morphology evolve over time and that this signal is nonlinear. Our work also shows that hydraulic model can be used to study the characteristics of floods and associated sedimentation through time to improve interpretations of sedimentary archives from floodplain lakes.

2 | STUDY AREA: TRINITY RIVER AND PORT OF LIBERTY LAKE, TEXAS

The Trinity River is a major drainage of the Texas Gulf Plain, with a drainage area of ~46,100 km^2 and mean annual discharge of 224 m^3/s (TWDB, 2022), which empties into the Gulf of Mexico via Trinity Bay (Phillips et al., 2004). Below the Livingston dam (completed in 1969), the Trinity River occupies a low-relief valley bottom bounded by Quaternary-age terraces (Blum & Aslan, 2006; Blum et al., 2002), with a riverbed below modern sea level (Phillips et al., 2005; Smith & Mohrig, 2017). The floodplain contains lakes formed during the Holocene and enlarged meander scrolls from channels occupying the floodplain during the Pleistocene (Phillips & Slattery, 2008; Phillips et al., 2005). Flooding associated with precipitation from Hurricane Harvey in August 2017 resulted in the largest annual peak flow event on the Trinity River at Liberty since 1995 (USGS, 2022). Harvey-induced flooding inundated large areas of the Trinity River floodplain, and mobilized and deposited large amounts of sediment (Blake & Zelinsky, 2018).

Our study focuses on a floodplain lake located on the southwest border of Liberty, Texas, which is referred to herein as Port of Liberty Lake (Figure 1). Port of Liberty Lake has an area of ~0.4 km^2 and is located ~85 km downstream of the Livingstone dam and ~3 km downstream of a USGS stream gauge (ID 08067000) (USGS, 2022).

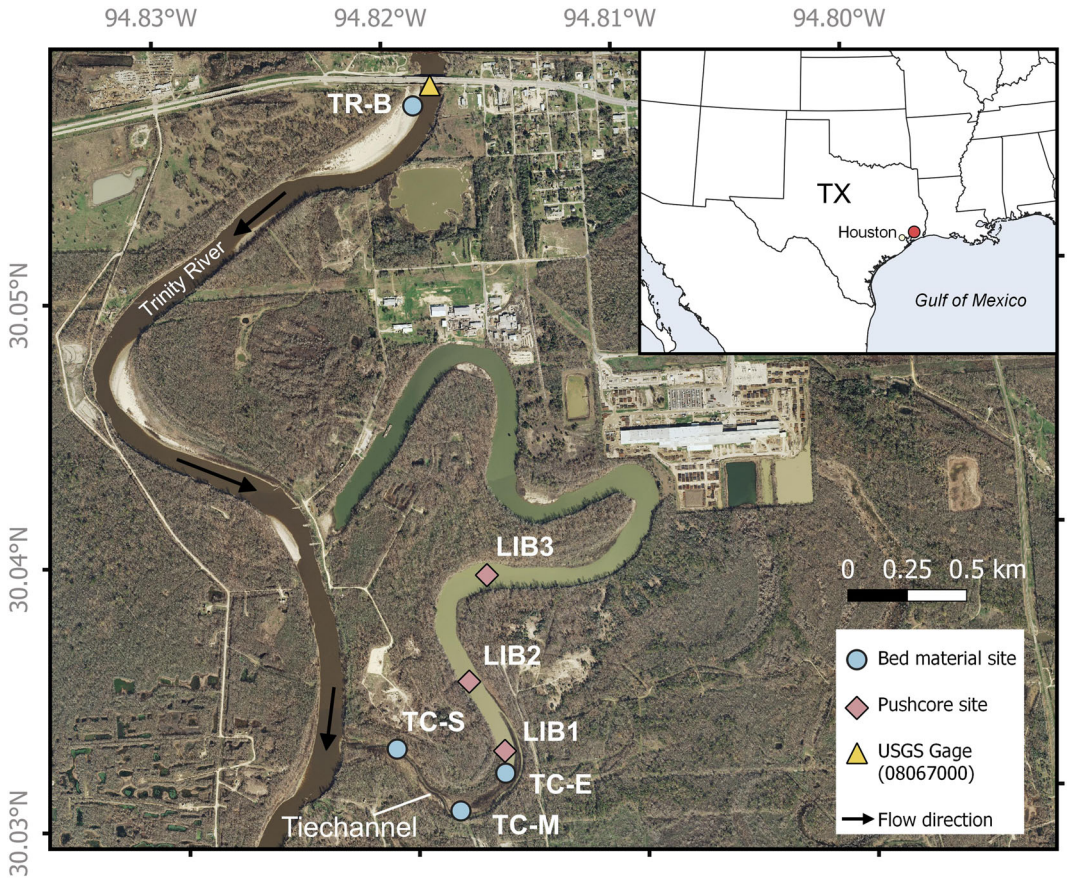

FIGURE 1 Surface sample (blue circles) and sediment core (red diamonds) locations around port of liberty Lake and Trinity River near Liberty, Texas [Color figure can be viewed at wileyonlinelibrary.com]

Based on historical USGS maps, the floodplain lake formed through a neck cut-off event between 1984 and 1986 (USGS HTMC, 1984, 1986), which may have been influenced by the construction of an embankment and road (Port Drive) that cut off the upstream arm of the lake from the river. The lake behaves as what Citterio and Piégay (2009) refer to as a backwater lake, where water from the main river channel primarily enters the floodplain lake through the downstream arm because the embankment prevents water from entering through the upstream arm, as opposed to a lotic lake, where water enters via the upstream arm. Backwater lakes typically display a sediment gradient with thick deposits in the downstream lake arm, and little sediment accumulation in the upstream lake arm (Citterio & Piégay, 2009). The sandy point bars at the downstream limb of the Port of Liberty Lake support the inference that it is backwater lake (Supporting Information Figure S1). The Port of Liberty Lake represents a typical oxbow lake in the early stages of the abandoned phase, where an active tie-channel directs flow into the lake during high water events.

3 | DATA AND METHODS

3.1 | Hydraulic modelling

To simulate inundation and flow velocities in the floodplain lake during flooding associated with precipitation from Hurricane Harvey (26–30 August), we employed the HEC-RAS 6.1 hydraulic modelling platform developed by the US Army Corps of Engineers (Brunner, 2021a). We chose HEC-RAS for its ability to simulate processes on different floodplain geomorphologies that can be manipulated through the internal GIS interface RASMapper (Yalcin, 2020). We ran our simulation using the HEC-RAS 2D model to simulate overbank flow through a floodplain lake without predetermining the overflow locations (Quirogaa et al., 2016). The 2D HEC-RAS model solves the Saint-Venant equations through an implicit finite volume (IFV) algorithm in an unstructured computational mesh (Brunner, 2021a; Kumar et al., 2020). In RASMapper we generated an initial structured mesh with 25 m grid cells in the flow area, which we refined with ~15 m grid cells for the river, lake, and tie-channel (Supporting Information Figure S2). Our unstructured mesh was further refined by adding breaklines along the banks of the river and lake, as well as other areas of rapid elevation change. Breaklines ensure a proper representation of topographic features and prevent water from 'leaking' between cells unrealistically in the simulation.

We ran an unsteady flow simulation based on the stage hydrograph from USGS gauge 08067000 at Liberty for the period 18 August to 8 September to assess flow velocity and sedimentation processes during the flood crest following Hurricane Harvey (Figure 3c). Besides the initially unsteady flow simulation developed and calibrated using the floodplain topography and lake bathymetry collected in 2017 pre Harvey, we also created modified plug-bar and lakebed elevations to develop a series of alternative bathymetric scenarios, described in Section 3.2. The upstream boundary condition in all scenarios was provided by the river stage hydrograph measured at the streamflow gauge of the Trinity River at Liberty. A digital elevation model

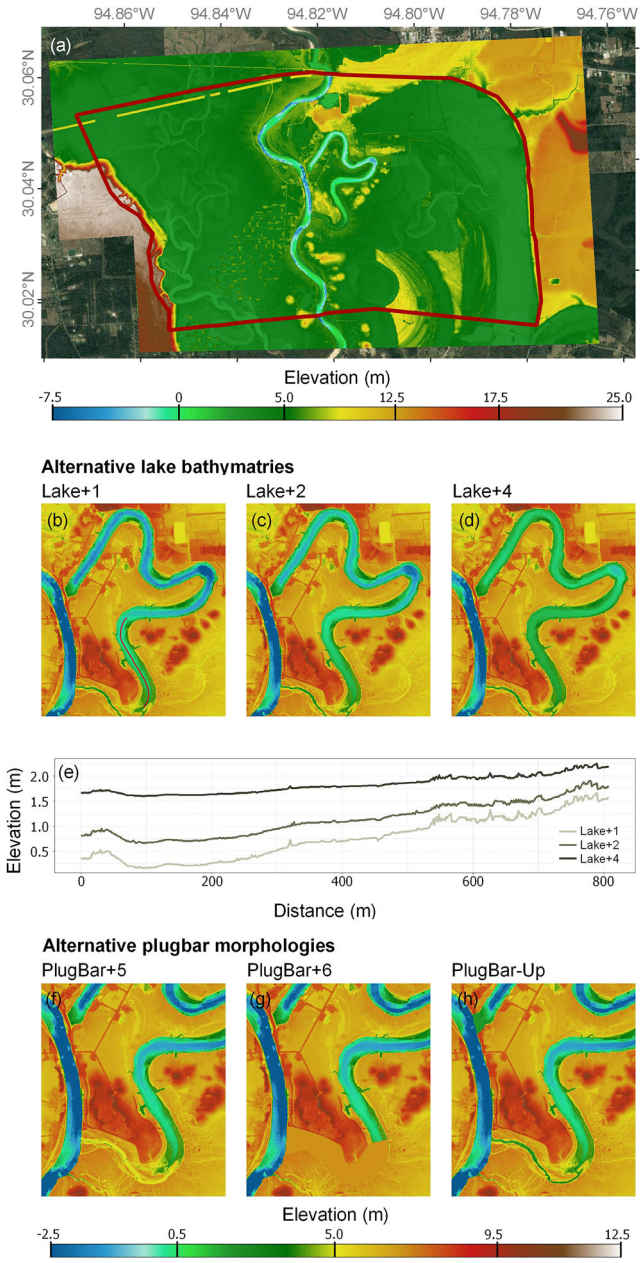

FIGURE 2 Bathymetry maps for different hydraulic model simulations. (a) Lidar data StratMap (2017) combined with bathymetry measurements of the Trinity River and Port of Liberty Lake collected by the Trinity River Authority. (b–d) Alternative lake bathymetry data created from a GIS; scenario Lake+1, Lake+2, and Lake+4, respectively. (e) Elevation profiles along the downstream lake arm of the bathymetries in scenario Lake+1, Lake+2 and Lake+4. (f–h) Alternative plug-bar geometries data created from a GIS; scenario PlugBar+5, PlugBar+6, and PlugBar-Up, respectively [Color figure can be viewed at wileyonlinelibrary.com]

(DEM)-derived normal depth boundary condition was used for both the downstream river (friction slope = 0.0075) and floodplain (friction slope = 0.005) boundaries to ensure that water could move out of the system (Supporting Information Figure S2). To classify land use types, we used the National Land Cover Database 2016 products (Dewitz, 2019) and the associated Manning's roughness values suggested by the HEC-RAS manual (Brunner, 2021b). To achieve model stability, the timestep for each model iteration was determined through the Courant–Friedrichs–Lewy condition (Equation 1), where T is the computational time step (s), x is the average cell size (m), V is the flood wave velocity (m/s), and C is the Courant number. If we assume x to be 25 m and the maximum V to be 5 m/s, we find a T of approximately 5 s (Brunner, 2021b; Shustikova et al., 2019):

$$\Delta T \leq \frac{\Delta x}{V} \ (\text{with } C = 1.0). \tag{1}$$

With this time step, the Courant value remains <0.5 in the lake and floodplain and <1.5 in the river, which we determine to be stable (Brunner, 2021a). We calibrated the model by varying the Manning's roughness values of the river around Manning's values suggested by the HEC-RAS manual, and the slope value at the downstream boundary to match the discharge values measured by the streamflow gauge at Liberty. From a sensitivity analysis we found that, of the two variables just for calibrating, simulated discharge is primarily affected by the roughness values. Missing discharge measurements ($n = 9$) from before and after the flood peak were reconstructed using a rating curve based on Trinity River discharges levels below 1700 m^3/s during the period 1996–2021 (Supporting Information Figure S3).

3.2 | Bathymetric data and scenarios

The computations in our hydraulic model are based on combined topographic data for the floodplain in our study area with bathymetric data of the river and floodplain lake. The topographic data consist of a 0.5 m resolution DEM based on ground LIDAR data provided from the Texas Strategic Mapping Program (StratMap, 2017), whereas bathymetry data for the Trinity River and Port of Liberty Lake were collected and made available by the Trinity River Authority in 2017 prior to the landfall of Hurricane Harvey. The bathymetric data were provided as a point-cloud with a vertical accuracy of 0.1 m and were interpolated using an inverse distance weighting (IDW) algorithm in QGIS to convert into raster format with 0.5 m resolution. The topographic and bathymetric datasets were merged into a terrain model in RASMapper after being converted to the same vertical datum. The bathymetric dataset did not include the bridge features at the upstream end of the study area where the stream gauge that provides upstream boundary conditions is located, so elevations were increased around bridge pillars to mimic these obstructions in the river.

To examine the changes in flow velocities and sedimentation regime as floodplain lakes infill and evolve, we developed a series of alternative bathymetric scenarios (Figure 2b,c). First, we constructed a set of three scenarios with a raised lakebed with a maximum modification elevation of 1, 2, and 4 m above the original bathymetry (respectively +1, +2, and +4). We increased the lakebed elevation of the original DEM using the raster calculator in QGIS. Sediment accumulation within the lake varies depending on depth, so we used a sigmoid function in which elevation changes are greatest in the deepest areas of the lake, but zero around the banks (Equation 2):

$$\text{Modification elevation} = \frac{1}{\frac{1}{\text{Maximum modification elevation}} + 3^{\left(\frac{\text{Lake depth}}{1.5} - C\right)}} \tag{2}$$

where Modification elevation is the height added to each grid cell of the lake, Maximum modification elevation is the largest desired

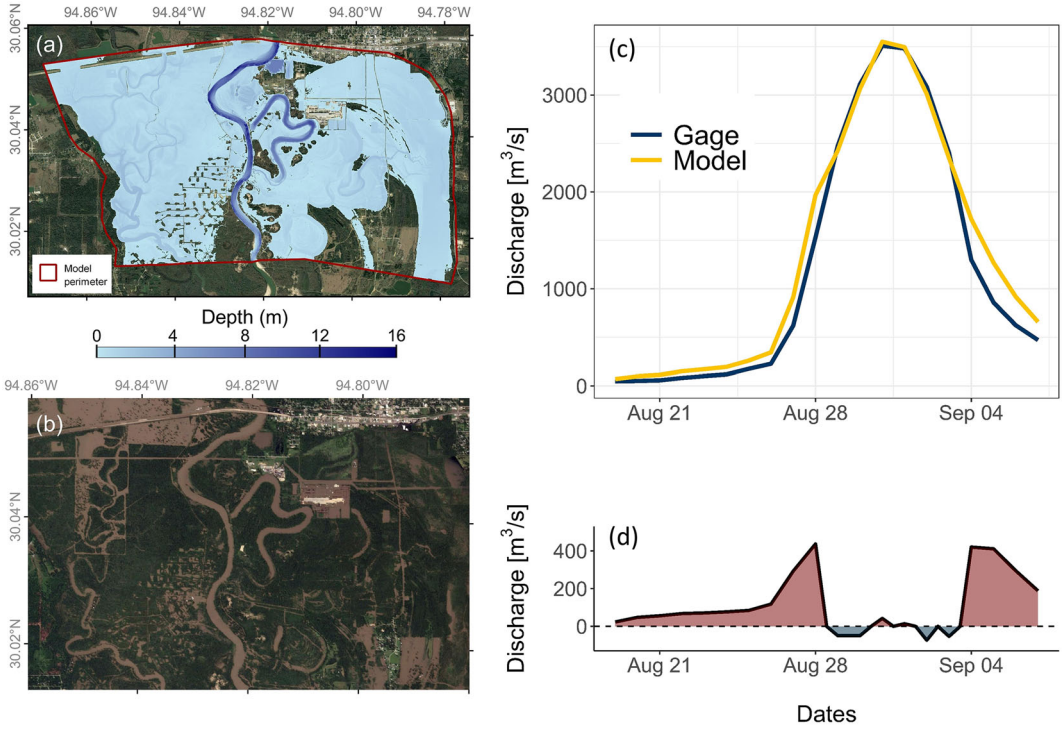

FIGURE 3 Hydraulic model output compared to observed data during the Hurricane Harvey floods: (a) simulated inundation depth during peak flow on 30 August 2017; (b) satellite imagery during the Hurricane Harvey floods on 31 August 2017, from Google Earth (satellite by Maxar technologies); (c) simulated and observed discharge over the simulation period at the USGS gauge 08067000; (d) modelled discharge minus observed discharge data over the simulation period [Color figure can be viewed at wileyonlinelibrary.com]

elevation change, *C* is a bathymetry depth-specific constant (0, 0.5, 1, respectively, for +1, +2, and +4), and Lake depth is the depth at the grid cell in the original bathymetry. Additionally, we created three alternative scenarios in which we modified the elevation of the plug-bar: (1) a partially infilled tie-channel (PlugBar+5); (2) a completely filled-in tie-channel (PlugBar+6); (3) original downstream tie-channel but without the embankment at the upstream lake limb (PlugBar-Up). Each of these alternative bathymetric scenarios were applied to the unsteady flow analyses described above, resulting in a total of seven scenarios including the original bathymetry.

3.3 | Sediment sampling and coring

To examine sediment mobilization and deposition after Hurricane Harvey, we collected sediment samples from a point-bar along the main Trinity River channel, at three locations along the tie-channel, and three sediment cores from the lake bottom along a transect of the downstream arm of Port of Liberty Lake (Figure 1). Sediment cores were collected in July 2021 using a rod-deployed piston coring system with a clear polycarbonate tube that allowed us to retain the sediment–water interface. Cores were collected at the end of the downstream lake arm (LIB1), ~350 m upstream from the tie-channel exit (LIB2), and at the lowermost bend in the lake ~800 m upstream from the tie-channel exit (LIB3). Coring locations were chosen based on preliminary hydraulic simulations that showed a drop in floodwater flow velocities beyond the location of LIB2. Sediment cores were transported back to Northeastern University, split lengthwise, described, photographed, and kept in cold storage.

We performed a grain-size analysis at 0.01 m resolution on the top 0.80 m of each core to identify the texture and thickness of coarse-grained deposits associated with recent flooding due to Hurricane Harvey. Each sediment subsample was pre-treated with 10 mL of 30% H_2O_2 to remove organic matter (van Hengstum et al., 2007) and 10 mL of dispersant (0.5% sodium hexametaphosphate) and mixed for 5–15 min on an orbital plate shaker before grain-size analysis using a Malvern Mastersizer 2000-LV laser diffraction particle size analyser (Vasskog et al., 2016). We unmixed the grain-size distributions in each core into different populations using end-member modelling (EMM) in the EMMAgeo package in RStudio (Dietze & Dietze, 2019). The coarsest end-members and the 90th percentile of the grain-size distribution (D_{90}) were used to identify coarse-grained event-beds that are deposited during extreme floods (Munoz et al., 2018; Toonen et al., 2015).

4 | RESULTS

4.1 | Hydraulic modelling

The hydraulic model successfully simulates the peak discharge magnitudes observed at the upstream gauge (Trinity River at Liberty), and matches the inundation extent observed from satellite imagery at the height of the flooding (31 August 2017) from Hurricane Harvey (Figure 3). The simulated river discharges during peak flow at the upstream boundary of our simulation (3551 m^3/s) are similar to those observed at the stream gauge (3510 m^3/s), with a difference of 41 m^3/s (~1%) (Figure 3c). The largest absolute differences between simulated and observed discharges occur prior to and following the

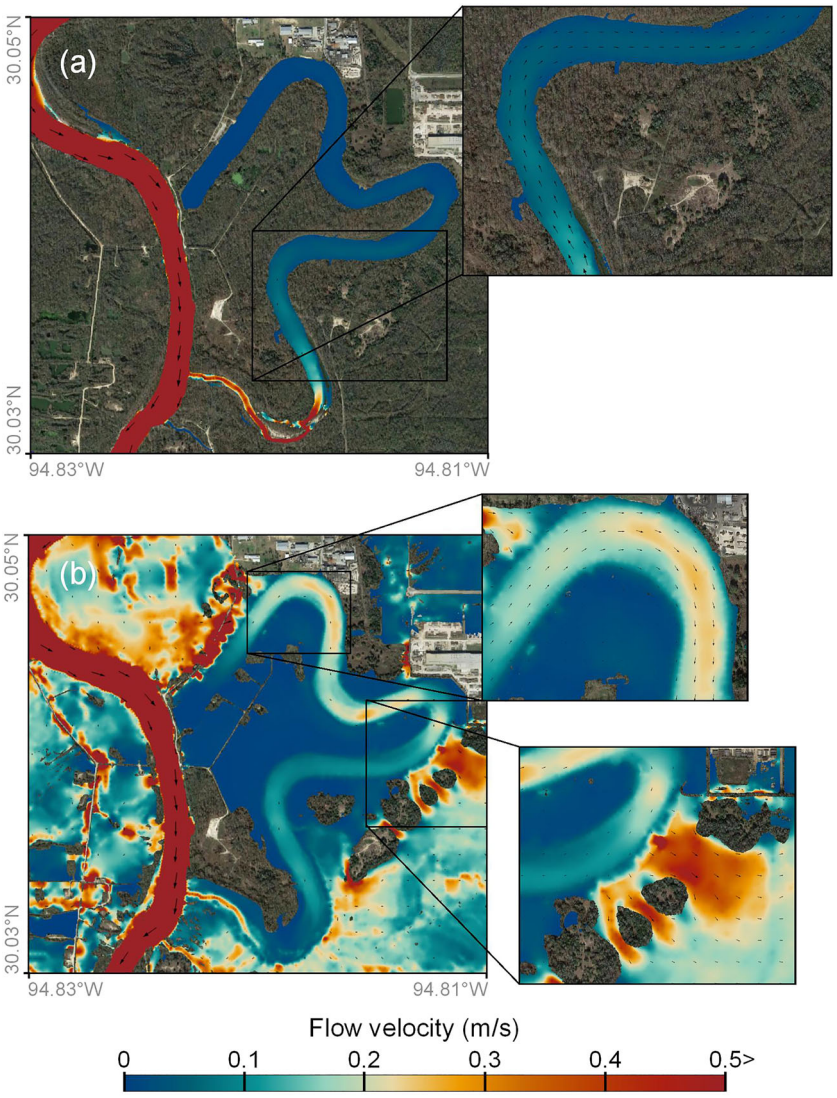

FIGURE 4 Simulated flow velocities and directions when (a) floodwater discharges into the lake via the tie-channel on 27 August 2017 at 09:00 CST, and when (b) discharge in the river crests on 31 August 2017 at 03:00 CST [Color figure can be viewed at wileyonlinelibrary.com]

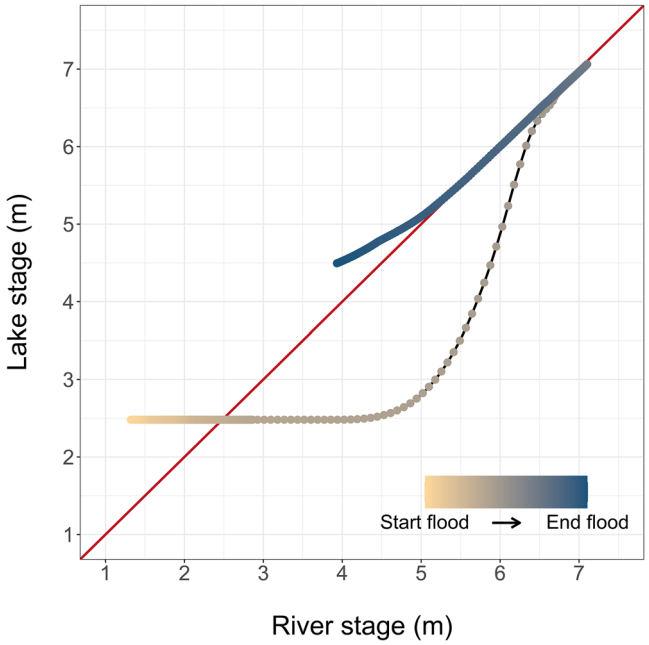

FIGURE 5 Hydrological connectivity between the lake in the downstream lake arm and river in the centre of the river at the elevation of the tie-channel [Color figure can be viewed at wileyonlinelibrary.com]

discharge peak on 24 August (436 m^3/s; 22% difference) and 4 September (420 m^3/s; 24% difference), suggesting that flows recede faster in the observed hydrograph than in the simulation (Figure 3c). The total root mean square error of the model is 200 m^3/s and the Nash–Sutcliffe efficiency (i.e., 1 minus the ratio of the error variance of the model and the observed discharges) is 0.97 (Beven, 2012). We also compared the simulated extent of floodplain inundation to remotely sensed imagery on 31 August 2017 (Figure 3b). We also observe a similar spatial pattern of inundation between the simulation (Figure 3a) and observations (Figure 3b), with dry areas situated between the Port of Liberty Lake and Trinity River and the southeast area of the model domain.

The hydraulic model shows that water from the river is fed to the lake predominantly via the tie-channel that connects the river to the downstream lake arm (Figure 4a) and that flow in the lake is directed upstream. Lake levels are first elevated by the rising flood peak on 26 August (2:00 pm CST) as river stage around the tie-channel entrance exceeds 4.0 m, the hydrological connectivity threshold of Port of Liberty Lake in its current state (Figure 5). As the flood reaches its crest on 27 August, water levels along the active and abandoned channel exceed the natural levee causing inundation to extend across ~80% of the floodplain. Similarly, the area along the outer bank of the

floodplain lake is inundated via overbank flooding of the lake; however, higher elevations and a road prevent flood water from flowing into the lake through the convex bank. In contrast, waters flow into the upstream lake limb via the floodplain, causing a reversal of flow direction in the lake (Figure 4b). Lake levels reach a maximum of 7.1 m on 31 August (7:00 am CST) at the same time as the flood crest in the river at 3550 m^3/s. Following this flood crest, inundation of the floodplain and floodplain lake gradually recedes and flow reverses through the tie-channel (Supporting Information Figure S4).

Flow velocity time series at different locations in the river and floodplain lake exhibit a nonlinear relationship between river discharge and flow velocity in the floodplain lake (Figure 6). Simulated flow velocities across the tie-channel and lake initially increase following the establishment of hydrological connectivity (Figure 6). Flow velocities are greatest in the narrowest section of the tie-channel (0.5–1.5 m/s) and slow down to <0.5 m/s where the tie-channel empties into the lake. Within the lake itself, flow velocities decrease with distance from the tie-channel and towards the lake banks. This first peak in flow velocities is greatest where the tie-channel connects to the lake (1.6 m/s), while flow velocities in other parts of the tie-channel do not exceed 0.6 m/s (Figure 6). Flow velocities decrease rapidly to 0.36 m/s where the tie-channel empties into the lake and decrease further to 0.05 m/s at 850 m from the tie-channel (Figure 4a). When river discharge peaks and floodwater flow into the upstream lake arm from the floodplain and out of the downstream lake arm, flow velocity increases again at all points resulting in a second velocity peak. However, the direction of flow is reversed in the floodplain lake (Figure 4b), causing the amplitude of the second peaks to be greater further from the tie-channel (Figure 6b). For example, the largest velocities (0.11 m/s) occur in the lake itself where floodwaters spill out onto the surrounding floodplain, with relatively low flow velocities at the tie-channel outlet (0.06 m/s). Flow velocities in the tie-channel remain high (0.30 m/s) (28 August to 4 September) as water continues to flow in from the river (Figure 4b) or out of the lake into the river during the flood crest.

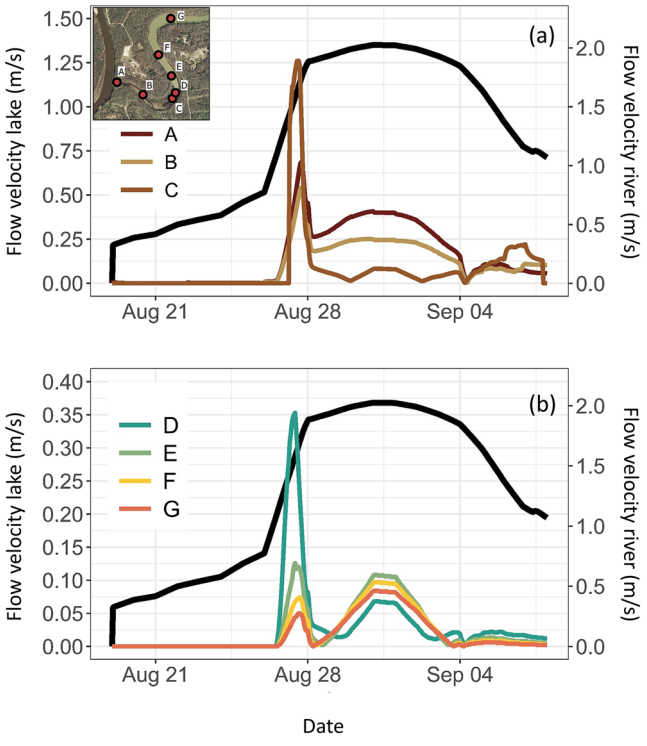

FIGURE 6 Flow velocities time series from several points in (a) the tie-channel and (b) the downstream lake arm. The black line indicates flow velocities in the centre of the river at the height of the tie-channel [Color figure can be viewed at wileyonlinelibrary.com]

4.2 | Sediment sampling and analysis

We identified coarse-grained deposits at the top of the three sediment cores collected along the downstream arm of Port of Liberty Lake that are consistent with accumulation resulting from the Hurricane Harvey floods (Figure 7). The peak discharge levels following the landfall of Hurricane Harvey in 2017 (3510 m^3/s) has not been exceeded since 1995 (3822 m^3/s), so it is unlikely that the uppermost coarse-grained deposits in Port of Liberty Lake would be the result of another event. Moreover, the observed lake depths in 2021 at the LIB1 coring site are ~0.5 m shallower than those recorded in the 2017 bathymetry survey prior to Hurricane Harvey. This difference is larger than the vertical accuracy of the 2017 survey and corresponds to the sediment thickness we attribute to deposits from Hurricane Harvey. The uppermost deposits in the cores characterized by a thick layer of medium- to fine-sands represent the coarse flood sediments typical of floodplain lakes in the abandoned stage (Toonen et al., 2012).

Grain-size distributions of the sediment cores show that the uppermost deposits are coarser than underlying material, and that these uppermost deposits decrease in thickness and grain size and with increased distance from the tie-channel (Figure 7). End-member (EM) modelling for each core results in three distinct end-member populations, where EM3 represents an extreme flood grain-size distribution with a left skew and narrow peak around 100 μm (Toonen et al., 2015), and dominates the uppermost deposits in all three cores. Adjacent to the tie-channel, core LIB1 has a mean D90 value of 220 μm from 0 to 0.48 m, which then drops to 78.5 μm deeper in the core. Further from the tie-channel, core LIB2 has a mean D90 of 113 μm from 0 to 0.12 m, while core LIB3 has a mean D90 from 0 to 0.04 m of 47 μm. The thinning and finning with distance from the tie-channel of the coarse-grained Hurricane Harvey deposits in the uppermost section of the core is consistent with the flow velocity profiles generated by our hydraulic model for this same event. Although the EM3 curves all represent the coarsest sediment population within their core, we do observe notable differences between the three EM3 populations. As we move away from the tie-channel, the grain-size distribution of EM3 shifts towards smaller grain-size values (peaks at 153 μm, 71 μm, 29 μm) and becomes narrower. These differences imply that the core closest to the tie-channel consists of sediments that can also be found further—and are captured in, for example, EM1 and EM2—out in the lake, but that the coarsest sediments are primarily deposited at the lake entrance.

A comparison between grain-size distributions of lake-bottom sediments and sediments collected from the tie-channel and active river channel shows that sediments deposited in the lake during an extreme flood reflect sorted sediments in the tie-channel (Figure 8). The grain-size distribution of tie-channel sediment closest to the floodplain lake (TC-E) (Figure 8c) shares a mode with the point-bar sediments (TR-B) at ~174 μm (Figure 8d), but TC-E has a greater percentage of coarse material. In contrast, tie-channel sediments closer

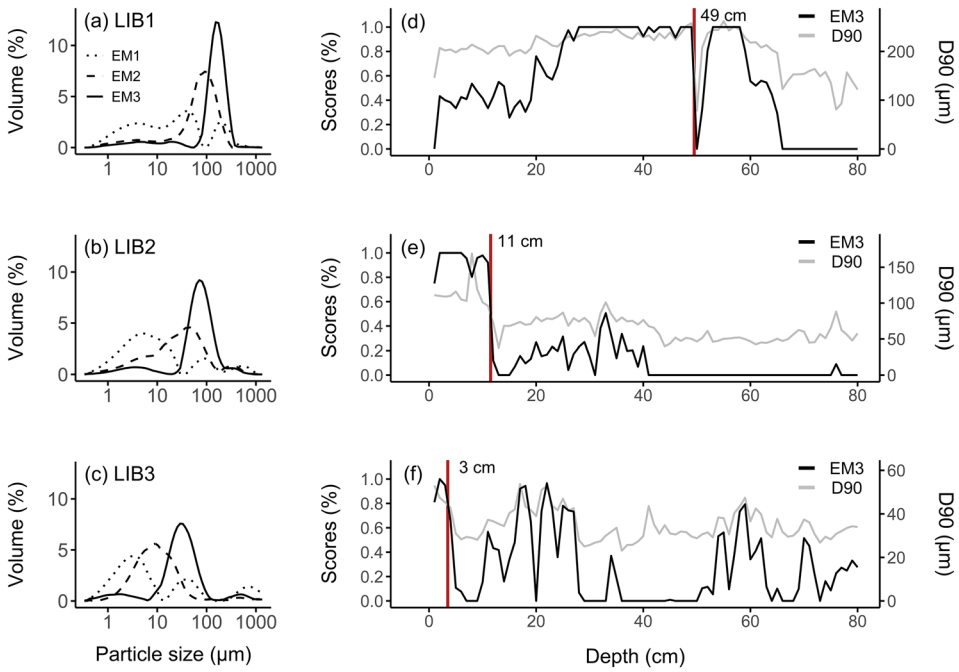

FIGURE 7 Grain-size populations from an end-member model and grain-size indicator profiles for three sediment cores from the Port of Liberty Lake. (a–c) The three distinct grain-size populations constructed in an end member model for the cores (a) LIB1, (b) LIB2, and (c) LIB3. (d–f) The black lines denote the relative contribution (score) of the coarsest end-member population (EM3) to each sample in cores (d) LIB1, (e) LIB2, and (f) LIB3. The grey lines denote the 90th percentile of the grain-size distribution of each sample. The red line denotes the depth of Hurricane Harvey sediment deposits based on the drop in the D90 value below 60 μm and visual inspection of the cores [Color figure can be viewed at wileyonlinelibrary.com]

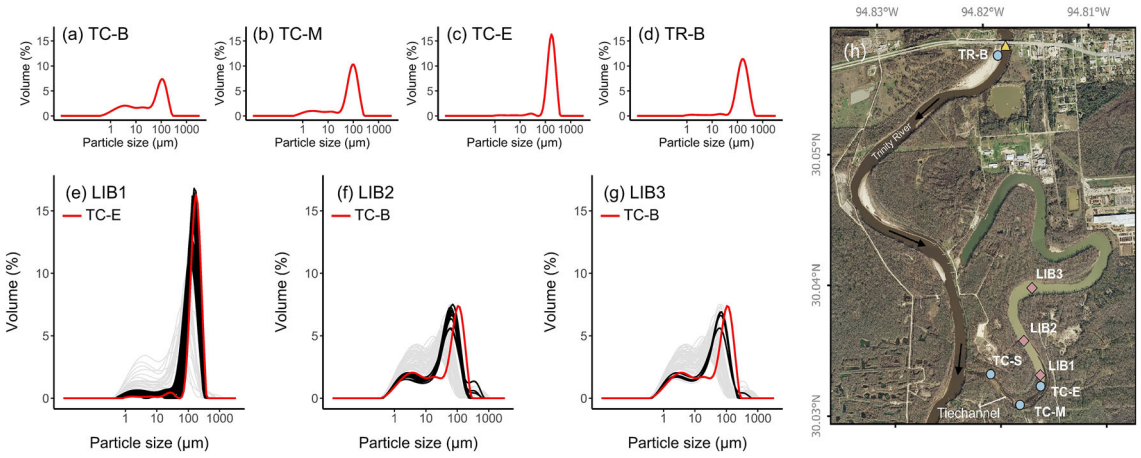

FIGURE 8 Grain-size distributions of sediments collected from (a–c) the tie-channel (TC-B, TC-M, and TC-E), (d) a point-bar in the Trinity River (TR-B), and (e–g) the lake bottom. (e–g) Black lines denote grain-size distributions from Hurricane Harvey sediment deposits. Grey lines denote grain-size distributions from non-Harvey sediment deposits [Color figure can be viewed at wileyonlinelibrary.com]

to the river (TC-B and TC-M) have a mode at ~104 μm (Figure 8a,b), and contain a higher percentage of finer material relative to TR-B and TC-E. These grain-size distribution patterns imply that the suspended sediments in the river are sorted within the tie-channel as floodwaters recede. The reversal of flow through the tie-channel as discharge recedes from the lake causes finer-grained material to be transported and deposited back closer to the river side of the tie-channel. A comparison between the lake-bottom deposits to the sediments in the tie-channel shows a similar sorting occurs in the lake itself (Figure 8e,g). Finer-grained sediments are carried further into the lake, causing a larger share of fine grain-sizes in cores further from the tie-channel (LIB2 and LIB3) relative to the core closest to tie-channel (LIB1).

4.3 | Alternative floodplain bathymetries

To examine the influence of floodplain lake evolution on flow velocity patterns, we developed a series of alternative bathymetries that vary plug-bar geometry and lake depth. First, we examined two scenarios with a matured plug-bar: (i) PlugBar+5, where the tie-channel has been filled up to 5 m; and (ii) PlugBar+6, where the entire tie-channel is filled up to 6 m to match the elevation of the surrounding floodplain (Figure 2f,g). These modifications serve to reduce hydrological connectivity of the lake, and imply that as the plug-bar matures higher river stages are required to transfer floodwaters and sediments from the river to the lake (Figure 9). In our simulations, the river stage at which the lake floods in the original tie-channel bathymetry is 4 m, while for scenario PlugBar+5 it is 5.3 m and for PlugBar+6 it is 6.6 m. In all scenarios, lake level rises to 7.2 m to match those of the river. Lake levels drop as river stage decreases following the flood crest, stabilizing at 4.5 m for the original bathymetry, 5.2 m for PlugBar+5, and 6.0 m for PlugBar+6, reflecting the importance of plug-bar elevation in mediating the transfer of water and sediments between the river and lake during flood and non-flood conditions. These simulations also show that plug-bar elevation influences flow velocity through the lake such that a completely infilled plug-bar (PlugBar+6 scenario) attenuates the initial burst of floodwaters and only allows floodwaters into the lake via overbank flow across the floodplain (Figure 9c).

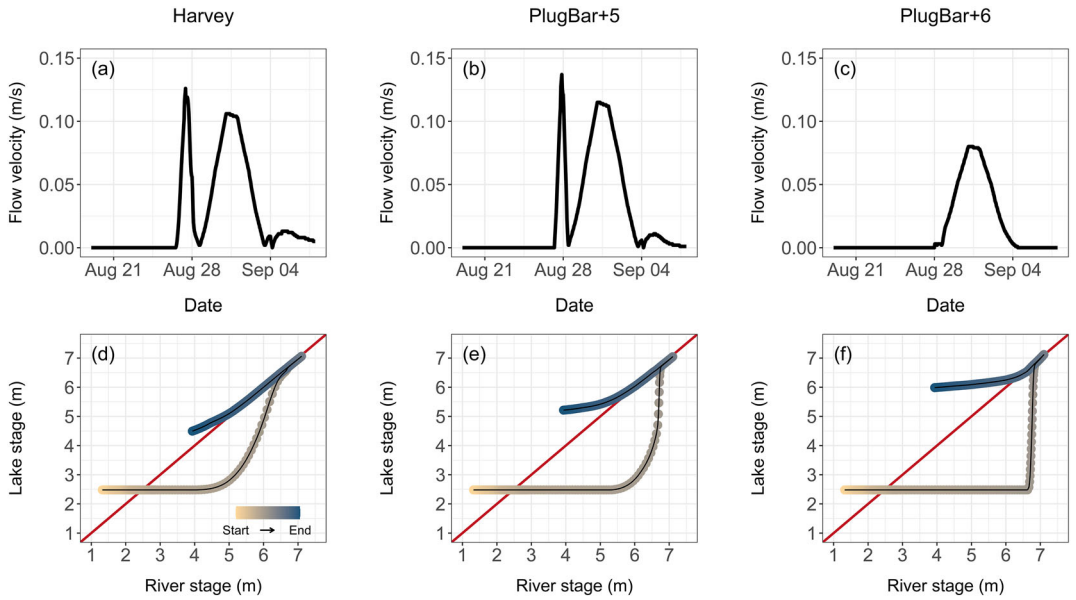

FIGURE 9 Hydraulic model simulation results for scenarios with alternative bathymetries focused on plug-bar elevation: (a–c) flow velocity in the lake over the simulation period for (a) the original lake bathymetry, (b) PlugBar+5, and (c) Plugbar+6 scenarios; (d–f) hydrological connectivity between the lake and river for (d) the original lake bathymetry, (e) PlugBar+5, and (f) Plugbar+6 scenarios [Color figure can be viewed at wileyonlinelibrary.com]

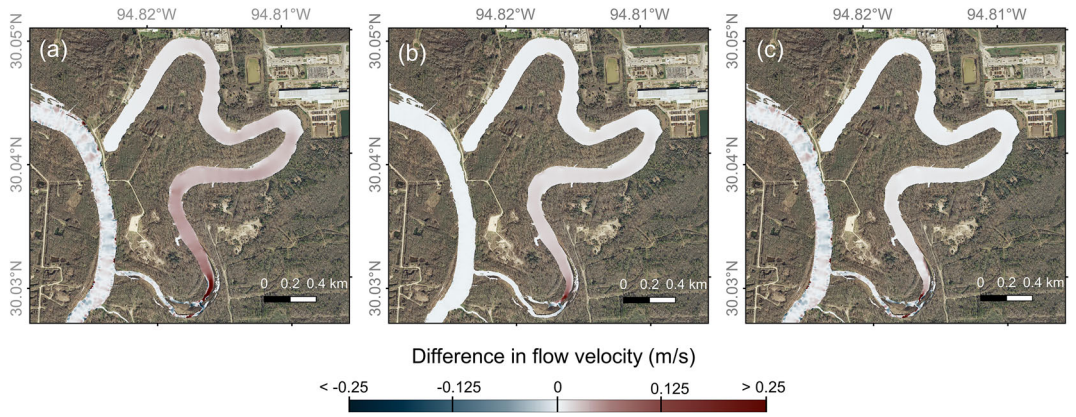

FIGURE 10 Hydraulic model simulations for scenarios with alternative lake bathymetries: (a) difference between flow velocities for the Lake +4 bathymetry minus the original bathymetry; (b) Lake+2 bathymetry; and (c) Lake+1 bathymetry [Color figure can be viewed at wileyonlinelibrary.com]

Next, we examined changes in flow velocities for three scenarios with floodplain lake infilling, Lake+1, Lake+2, and Lake+4, where the lakebed is raised by a maximum of 1, 2, and 4 m (Figure 2). These simulations show that as the lake becomes shallower initial peak flow velocities extend further into the lake. For scenario Lake+1, the change in flow velocity relative to the original bathymetry is minor (Figure 10c), but for scenarios Lake+2 and Lake+4 flow velocities increase by 0.10–0.15 m/s out to the middle of the lake (Figure 10a,b). The general pattern in flow velocity time series at multiple points along the lake does not change across scenarios, with an initial increase in flow velocity when water first enters the lake, followed by a second longer increase in flow velocities as river discharge crests (Supporting Information Figure S5). However, peak flow velocities increase as the lake infills with a difference of 0.34 m/s between the Lake+4 scenario and the original bathymetry. These findings imply that coarser material would be transported further in a shallower floodplain lake, and that patterns of sedimentation in a floodplain lake will change as the lake evolves over time.

Finally, we examined flow velocities for scenario PlugBar-Up, where the embankment impeding hydrological connectivity at the upper arm is removed such that Port of Liberty Lake is no longer a backwater lake (Figure 2h). This scenario shows that, with an open upstream connection to the river, flow reverses towards a downstream direction and velocities increase throughout the lake such that the lake forms an anabranch of the river during an extreme flood. In contrast to the other scenarios examined, an open upper arm reduces the threshold for hydrological connectivity to 2.5 m (Figure 11b) and causes flow velocity patterns between the river and lake to be synchronous (Figure 11a). At peak river discharge, velocities are highest (0.50 m/s) in the upstream lake arm and decrease to 0.25 m/s in the downstream lake arm. These results document the sensitivity of floodplain lake hydrodynamics to plug-bar elevation and lake orientation, and imply that sedimentation in backwater floodplain lakes will differ from lakes with hydrological connectivity at their upper arm. Bed sediments are likely to be deposited more uniformly in the lake as they stay entrained in the higher flow velocities. This shows that

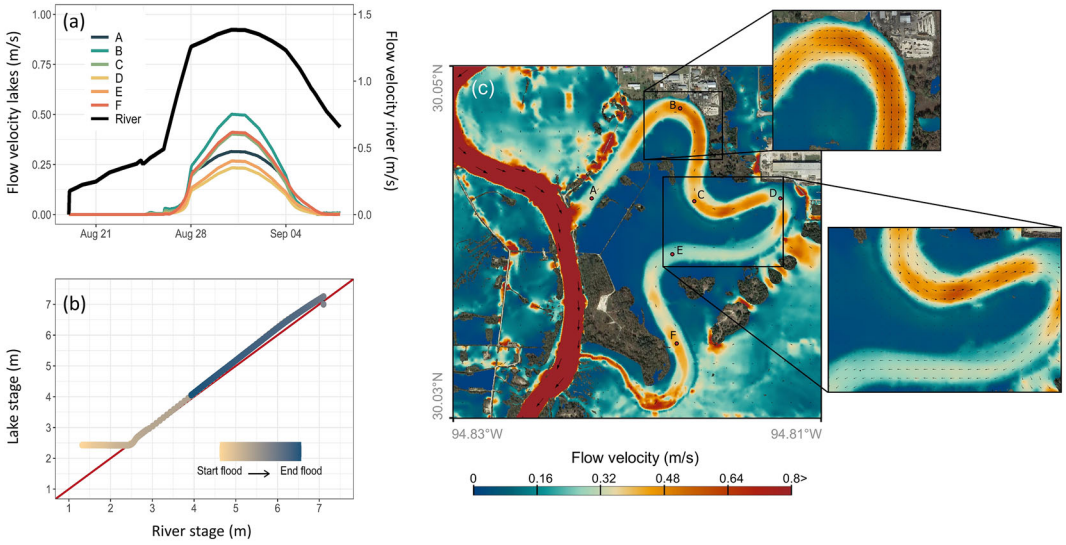

FIGURE 11 Hydraulic model simulation results for the PlugBar-Up scenario: (a) flow velocities for multiple locations throughout the lake (coloured lines; locations shown in panel c) and flow velocity in the river (black line); (b) hydrological connectivity between the lake and river in the PlugBar-Up scenario; (c) simulated flow velocities and directions (arrows) when river discharge in the river crests on 31 August 2017 at 01:00 CST [Color figure can be viewed at wileyonlinelibrary.com]

landforms around the lake such as plug-bars and lake geometry play an essential role in lake infilling and sediment deposition.

5 | DISCUSSION

In this study, we combine field-based sediment sampling with hydraulic modelling to examine inundation, flow velocity, and sedimentation patterns in a floodplain lake during an extreme flood event. Our hydraulic model developed using HEC-RAS accurately simulates the discharge and inundation extent of flooding that followed Hurricane Harvey in August 2017 based on observed river stage levels (Figure 3). Simulations of this extreme flood show that once floodwater attains a stage of 4 m hydrological connectivity is achieved, and floodwaters reach the lake via the tie-channel at the downstream lake arm (Figure 5). The initial pulse of floodwaters into the lake increases flow velocities throughout the lake, with the highest velocities in the tie-channel and downstream lake arm (Figure 4a). When the flood crests, flow velocities increase and flow direction changes as floodwaters enter the lake through the floodplain along the upstream arm and spill out across the floodplain (Figure 4b). Sediment samples collected from the tie-channel and lake bottom show that the initial pulse of floodwater erodes coarse-grained material from the tie-channel and transports it into the lake, where it is deposited as a coarse-grained bed that thins and fines with distance from the tie-channel (Figures 7 and 8). Model runs using alternative bathymetries for the same flood event demonstrate that flow velocities increase as the lake shallows through infilling, and that these higher velocities propagate further into the lake. Additional model runs with alternative plug-bar geometries demonstrate that the threshold for hydrological connectivity increases as the plug-bar elevation increases. Moreover, we show that flow velocities in a backwater floodplain lake (i.e., where hydrological connectivity occurs primarily through the downstream arm) are lower when compared to a situation where floodwaters can flow through both the upstream and downstream arms. Together, the sediment samples and hydraulic simulations provide key insights into how and why sedimentation proceeds in a floodplain lake after an extreme flood event. Furthermore, this work demonstrates that the parameters of theoretical models of floodplain lake evolution can also aid our interpretations of individual events from sedimentary archives from within these contexts.

5.1 | Theoretical models of floodplain lake sedimentation

Our findings support and build on key parameters of theoretical models describing long-term floodplain lake evolution (Gagliano & Howard, 1984; Toonen et al., 2012), by providing insights into the mechanisms that generate observed sedimentation patterns. The hydraulic simulations reproduce the expected behaviour of a young floodplain lake in its transitional phase with a developing plug-bar and lake shallowing as described by Toonen et al. (2012) during an extreme flood event. Plug-bar growth can be observed as flow velocities peak at the end of the downstream lake arm, but do not propagate into the lake, implying that deposition of coarse-grained sediments occurs around the lake entrance during this stage. Moreover, flow velocities reduce towards the banks of the lake, resulting in preferential deposition that narrows the lake (Douglas Shields & Abt, 1989). The sediment cores also reflect transitional floodplain lake fills (Toonen et al., 2012) and support the simulation results. The uppermost deposits in core LIB1 consist of thick (~0.4 m) coarse-grained (>200 μm) sediment, typical of a floodplain lake with a low plug-bar that allows water to flow in easily, while the uppermost coarse beds captured in the other cores winnow as distance from the plug-bar increases. We show that bed material samples from the tie-channel match these coarse-grained lakebed sediments, demonstrating that the tie-channel acts as the conveyor belt that brings water and coarse sediment to the lake entrance. The lack of thinly laminated layers below the uppermost coarse-grained deposits further supports that

the lake has not yet reached full abandonment from the river (Gagliano & Howard, 1984; Toonen et al., 2012). In short, the HEC-RAS software can be used to describe both the general patterns of floodplain lake evolution and the individual sediment signal after an extreme flood event.

The alternative bathymetry simulations further support observations and theoretical models that describe the transformation from the transitional lake phase to an abandoned floodplain lake with thinly laminated coarse sediment layers (Citterio & Piégay, 2009; Gagliano & Howard, 1984; Toonen et al., 2012). The hydraulic simulations show that, as the lake becomes shallower and narrower in the transitional phase, flow velocities extend further into the lake, which would result in more extensive transport of coarse-grained material into the lake. At the same time, increased plug-bar height increases the threshold for hydrological connectivity, creating a barrier that increasingly impedes sedimentation in the lake, except during the largest flood events. In these ways, lake and plug-bar infilling generate the laminated sedimentary fills that are characteristic of floodplain lakes in the abandoned stage (Bábek et al., 2008; Citterio & Piégay, 2009; Munoz et al., 2018). When floodwaters enter the lake via multiple entrances through overland flow across the floodplain instead of being only funnelled through the tie-channel, sedimentation will be more uniform across the lakebed (Hudson et al., 2012). In our simulations, however, elevated areas of the floodplain between the lake and river obstruct floodwaters (Figure 3a), implying that in-lake sedimentation patterns will also be influenced by floodplain morphology beyond the plug-bar and lake bathymetry, as examined in this study. Together, our simulations with alternative lake bathymetries show how the sediment signal from a given flood is contingent on progressive changes in the lake and floodplain morphology.

Finally, the PlugBar-Up simulation documents the differences in flow velocity patterns and inundation for floodplain lakes that receive floodwaters through a downstream entrance (backwater lakes) and those that receive floodwaters primarily through an upstream entrance (lotic lakes), and support observations of sedimentation patterns in these lakes (Figure 11) (Citterio & Piégay, 2009). In the hydraulic model, opening the upstream entrances increased the hydrological connectivity, overall flow velocities, and reversed the direction of flow in the lake (Figure 11). These simulations imply that coarse sediments in a lotic lake will either be distributed more homogeneously or flow out of the lake entirely, as lotic lakes exhibit reduced trapping efficiency relative to backwater lakes (Constantine et al., 2010). Observed sedimentation patterns support these inferences, where sedimentation in backwater lakes occurs primarily in the downstream lake arm, whereas in lotic lakes sedimentation is minimal and distributed more evenly across the lake because the lake acts as an anabranch of the active river channel (Citterio & Piégay, 2009). The trapping efficiency of lotic and backwater lakes will also be dependent on lake geometry, where straighter lakes with lower diversion angles allow flow velocities to remain high and limit sedimentation in the lake (Constantine et al., 2010). This is reflected by the reduced flow velocity in the lake bends, which suppresses sedimentation potential. Here, the hydraulic model allows us to decipher site-specific sedimentation patterns based on lake geometry and within the context of long-term floodplain lake evolution of lake models.

5.2 | Applications and implications

Our work demonstrates how hydraulic modelling can be applied to interpretations of individual events in sedimentary archives recovered from floodplain lakes by (i) guiding sample collection, (ii) identifying the hydrological connectivity threshold in current bathymetry, and (iii) quantifying the relation between river discharge and sediments deposited in the lake. To guide sampling collection, flow velocity simulations in a hydraulic model can be used to infer likely locations of erosion (i.e., where flow velocities are high) and deposition (i.e., where flow velocities are low), as well as locations where sediment might be disturbed or subject to reworking. Moreover, alternative lake bathymetries could be used to evaluate how patterns of erosion and deposition have changed over time using an approach similar to our development of the Lake+4, Lake+5, and Lake+6 scenarios. We also demonstrate how hydraulic modelling can identify the minimum river stage that results in floodplain lake sedimentation by simulating the flood of record. A similar exercise could be done with a staggered hypothetical hydrograph to identify when hydrological connectivity is reached and the sensitivity of flow velocities to different flood magnitudes.

This study outlines an advance in the use of hydraulic modelling on floodplains by relating flow velocities to sedimentation patterns in floodplain lakes, and the use of alternative bathymetries to evaluate the sensitivity of these patterns to lake evolution and infilling. Sediment samples from the lake bottom document how coarse-grained event beds are sorted within the lake during extreme flood events, demonstrating that these deposits thin and fine with distance from the tie-channel (Figure 7). Our findings show how flow velocity patterns change as the lake infills (Figure 10), implying that depositional patterns will change over time to generate foreset bedding via progradation across the lake arm (Figure 12). These findings are particularly relevant in the use of grain-size distributions to infer flood magnitudes (Jones et al., 2010; Wilhelm et al., 2019), because they imply that at a single core location the relationship between river discharge and grain size will be nonlinear and non-stationary. This relationship is nonlinear because flow velocities in the tie-channel and lake do not peak when river discharge crests. Instead, energy to erode material from the tie-channel is maximized during a pulse when floodwaters from the river initially flow into the lake. As a result, peak flow velocities in the tie-channel will be a function of tie-channel geometry, lake level immediately preceding the flood, and the rate of stage increase in the river at the onset of flooding. In addition to being nonlinear, the relationship between river discharge and grain size is non-stationary because, as the lakebed infills, high flow velocities extend further into the lake such that coarse-grained event beds will become thicker and coarser for a flood with a similar discharge. Additional changes to the tie-channel and plug-bar via infilling and vegetation succession will further alter the relationship between flood magnitudes and event bed properties. These findings do not negate prior work inferring flood magnitudes from grain-size distributions (Munoz et al., 2018; Toonen et al., 2015, 2019), but instead add nuance to these interpretations and point towards opportunities to reduce their uncertainties.

The application of alternative bathymetries in hydraulic modelling utilized in this study provides an avenue to improve on prior work estimating the hydrological characteristics of a flood from sediments.

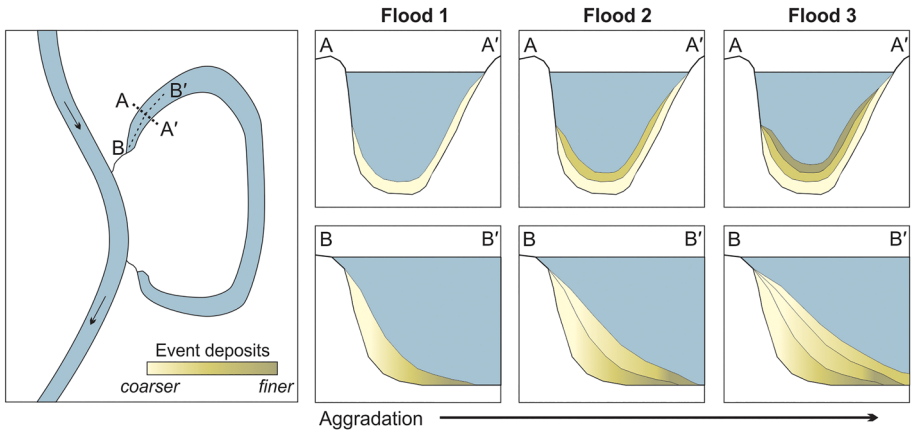

FIGURE 12 Conceptual diagram of the change in sediment deposition after flood events of the same magnitude as a result of floodplain lake evolution [Color figure can be viewed at wileyonlinelibrary.com]

The use of a linear model to estimate peak river discharge from grain-size distributions generates 1σ uncertainties of the order of 5–20% (Fuller et al., 2019; Munoz et al., 2018; Toonen et al., 2015, 2019), and these large uncertainties can be detrimental to the accuracy of flood frequency analysis (Reinders & Muñoz, 2021). To improve on these discharge estimates, an inverse-modelling approach could be used that simulates flow velocities and sedimentation patterns under different river discharge and bathymetric scenarios. Our work demonstrates how bathymetric scenarios can be developed using simple assumptions of infilling patterns, and these patterns could be constrained using sedimentation rates derived from sediment cores. For example, the sediment cores recovered in this study could be used to reconstruct lakebed morphology and prior to the Hurricane Harvey floods, or at earlier points in time, which could then be examined within a hydraulic model under a range of flood scenarios. The resulting flow velocity, sediment transport thresholds, and sediment distribution patterns could assist in the interpretation and analysis of the lake's observed sedimentary characteristics. Hydraulic models could also serve the analysis of sediment transport on floodplains more generally, for example by studying avulsions. The integration of sediment transport into hydraulic models, including in HEC-RAS 6, could further facilitate these efforts by simulating deposition resulting from a flood of a given magnitude. The integration of hydraulic models into palaeoflood hydrology has focused primarily on slackwater deposits in bedrock canyons, but our work implies that a similar approach could be applied in dynamic alluvial settings.

6 | CONCLUSIONS

Floodplain lakes constitute important stores of sediment (Asselman & Middelkoop, 1995; Phillips et al., 2004; Walling & Bradley, 1989), nutrients (Thoms, 2003), and pollution (Ciszewski & Grygar, 2016), yet the sedimentation patterns in these lakes are non-stationary and nonlinear due to changes in flow velocity patterns as lake geometry and floodplain topography evolve over time (Gagliano & Howard, 1984; Toonen et al., 2012). Therefore, existing models of floodplain lake evolution are not well suited to guide the interpretation of individual flood events in sedimentary records. In this study, we examine sedimentation and flow velocity patterns in a floodplain lake during a flood event by combining field-based sampling of flood deposits resulting from the extreme flooding in the wake of Hurricane Harvey with hydraulic model simulations of this event implemented in HEC-RAS. Our simulations demonstrate the mechanisms that result in the deposition of coarse-grained sediments in the floodplain lake via the tie-channel, and how these deposits thin and fine with distance from the tie-channel. We also use a series of hydraulic model simulations using alternative lake and plug-bar bathymetries to examine the sensitivity of flow velocity patterns to floodplain lake evolution and infilling. These modelling exercises imply that sedimentation patterns in floodplain lakes are highly sensitive to local floodplain geomorphology and lake evolution. Subsequently, the sediment signal of a particular flood will change over time due to the progressive infilling of the lake. Our findings build on theoretical models describing sedimentation in floodplain lakes (Gagliano & Howard, 1984; Toonen et al., 2012) by showing that numerical models such as HEC-RAS can provide a mechanistic understanding of observed sedimentation patterns and how these patterns change over time. We demonstrate how hydraulic modelling can aid in interpretations of individual events in sedimentary records in alluvial settings to improve reconstructions of ecological and hydrological dynamics in riverine environments.

ACKNOWLEDGEMENTS

The authors thank Paul Hudson, Auroop Ganguly, and Dick Bailey for valuable discussion and comments on this work. We also would like to thank the Trinity River Authority and, in particular, Webster Mangham for providing bathymetry data of the Trinity River at Liberty, Texas, and the Port of Liberty Lake. This project was supported by grants from the US National Science Foundation (EAR1804107 and EAR-1833200).

AUTHOR CONTRIBUTIONS

Joeri Reinders: conceptualization, methodology, investigation, resources, software, writing—initial draft, writing—reviewing and editing. **Richard Sullivan:** investigation, resources, writing—reviewing and editing **Tyler Winkler:** investigation, resources, writing—reviewing and editing. **Peter van Hengstum:** investigation, funding acquisition, writing—reviewing and editing **Edward Beighley:** software, writing—reviewing and editing **Samuel Munoz:** conceptualization, funding acquisition, supervision, writing—initial draft, writing—reviewing and editing.

DATA AVAILABILITY STATEMENT

Stage and discharge data in this study are available through the United States Geological Survey (USGS) Water Data for the Nation (https://waterdata.usgs.gov/nwis). The HEC-RAS model used for the analyses in this article is available from the corresponding author.

ORCID

Joeri B. Reinders https://orcid.org/0000-0002-9418-9881
Samuel E. Munoz https://orcid.org/0000-0002-0994-0483

REFERENCES

Amoros, C. & Bornette, G. (2002) Connectivity and biocomplexity in waterbodies of riverine floodplains. *Freshwater Biology*, 47(4), 761–776. Available from: https://doi.org/10.1046/j.1365-2427.2002.00905.x

Asselman, N.E.M. & Middelkoop, H. (1995) Floodplain sedimentation: Quantities, patterns and processes. *Earth Surface Processes and Landforms*, 20(6), 481–499. Available from: https://doi.org/10.1002/esp.3290200602

Bábek, O., Hilscherová, K., Nehyba, S., Zeman, J., Famera, M., Francu, J., et al. (2008) Contamination history of suspended river sediments accumulated in oxbow lakes over the last 25 years. *Journal of Soils and Sediments*, 8(3), 165–176. Available from: https://doi.org/10.1007/s11368-008-0002-8

Bartlein, P.J., Harrison, S.P., Brewer, S., Connor, S., Davis, B.A.S., Gajewski, K., et al. (2011) Pollen-based continental climate reconstructions at 6 and 21 ka: A global synthesis. *Climate Dynamics*, 37(3), 775–802.

Beven, K. (2012) Rainfall-Runoff Modelling: The Primer: Second Edition. In: *Rainfall-runoff modelling: The primer*, Second edition, Chichester, West Sussex: John Wiley & Sons. Available from: https://doi.org/10.1002/9781119951001

Bhattacharya, R., Hausmann, S., Hubeny, J.B., Gell, P. & Black, J.L. (2016) Ecological response to hydrological variability and catchment development: Insights from a shallow oxbow lake in lower Mississippi Valley, Arkansas. *Science of the Total Environment*, 569-570, 1087–1097. Available from: https://doi.org/10.1016/j.scitotenv.2016.06.174

Blake, E.S. & Zelinsky, D.A. (2018) National Hurricane Center Tropical Cyclone Report Hurricane Harvey. Available from: https://www.nhc.noaa.gov/data/tcr/AL092017_Harvey.pdf

Blum, M.D. & Aslan, A. (2006) Signatures of climate vs. sea-level change within incised valley-fill successions: Quaternary examples from the Texas Gulf Coast. *Sedimentary Geology*, 190(1-4), 177–211. Available from: https://doi.org/10.1016/j.sedgeo.2006.05.024

Blum, M.D., Carter, A.E., Zayac, T. & Goble, R. (2002) Middle Holocene Sea-level and evolution of the Gulf of Mexico coast (USA). *Journal of Coastal Research*, 36, 65–80. Available from: https://doi.org/10.2112/1551-5036-36.sp1.65

Brugam, R.B. & Munoz, S.E. (2018) A 1600-year record of human impacts on a floodplain lake in the Mississippi River valley. *Journal of Paleolimnology*, 60(3), 445–460. Available from: https://doi.org/10.1007/s10933-018-0033-0

Brunner, G.W. (2021a) HEC-RAS River Analysis System 2D Modeling User's Manual Version 6.0. US Army Corps of Engineers. Available from: https://www.hec.usace.army.mil/software/hec-ras/documentation/HEC-RAS_6.0_2D_Modeling_Users_Manual.pdf

Brunner, G.W. (2021b) HEC-RAS River Analysis System User's Manual Version 6.0. US Army Corps of Engineers. Available from: https://www.hec.usace.army.mil/software/hec-ras/documentation/HEC-RAS_6.0_Users_Manual.pdf

Ciszewski, D. & Grygar, T.M. (2016) A review of flood-related storage and remobilization of heavy metal pollutants in river systems. *Water, Air, and Soil Pollution*, 227(7), 239. Available from: https://doi.org/10.1007/s11270-016-2934-8

Citterio, A. & Piégay, H. (2009) Overbank sedimentation rates in former channel lakes: Characterization and control factors. *Sedimentology*, 56(2), 461–482. Available from: https://doi.org/10.1111/j.1365-3091.2008.00979.x

Constantine, J.A., Dunne, T., Piégay, H. & Mathias Kondolf, G. (2010) Controls on the alluviation of oxbow lakes by bed-material load along the Sacramento river, California. *Sedimentology*, 57(2), 389–407. Available from: https://doi.org/10.1111/j.1365-3091.2009.01084.x

Cooper, C.M. & McHenry, J.R. (1989) Sediment accumulation and its effects on a Mississippi River oxbow lake. *Environmental Geology and Water Sciences*, 13(1), 33–37. Available from: https://doi.org/10.1007/BF01666569

Dee, S.G., Russell, J.M., Morrill, C., Chen, Z. & Neary, A. (2018) PRYSM v2.0: A proxy system model for lacustrine archives. *Paleoceanography and Paleoclimatology.*, 33(11), 1250–1269. Available from: https://doi.org/10.1029/2018PA003413

Dewitz, J. (2019) National Land Cover Database (NLCD) 2016 products. U.S. Geological Survey 10.0.19.202/P96HHBIE.

Dietze, M. & Dietze, E. (2019) End-Member Modelling of Grain-Size Data. Available from: https://cran.r-project.org/web/packages/EMMAgeo/EMMAgeo.pdf

Douglas Shields, F. & Abt, S.R. (1989) Sediment deposition in cutoff meander bends and implications for effective management. *Regulated Rivers: Research & Management*, 4(4), 381–396. Available from: https://doi.org/10.1002/rrr.3450040406

Fisk, H.N. (1948) Fine-grained alluvial deposits and their effects on Mississippi River activity. *Corps of Engineers Vicksburg Miss*, 1(6), 591. Available from: https://doi.org/10.1086/625561

Fuller, I.C., Macklin, M.G., Toonen, W.H.J., Turner, J. & Norton, K. (2019) A 2000 year record of palaeofloods in a volcanically-reset catchment: Whanganui River, New Zealand. *Global and Planetary Change*, 181, 102981. Available from: https://doi.org/10.1016/j.gloplacha.2019.102981

Gagliano, S.M. & Howard, P.C. (1984) The neck cutoff oxbow lake cycle along the lower Mississippi River.

Gilli, A., Anselmetti, F.S., Glur, L. & Wirth, S.B. (2012) Lake Sediments as Archives of Recurrence Rates and Intensities of Past Flood Events. In: *Dating Torrential Processes on FAns and Cones*. Dordrecht: Springer. Available from:. https://doi.org/10.1007/978-94-007-4336-6_15

Hudson, P.F., Heitmuller, F.T. & Leitch, M.B. (2012) Hydrologic connectivity of oxbow lakes along the lower Guadalupe River, Texas: The influence of geomorphic and climatic controls on the "flood pulse concept". *Journal of Hydrology*, 414-415, 174–183. Available from: https://doi.org/10.1016/j.jhydrol.2011.10.029

Jones, A.F., Lewin, J. & Macklin, M.G. (2010) Flood series data for the later holocene: Available approaches, potential and limitations from UK alluvial sediments. *Holocene*, 20(7), 1123–1135. Available from: https://doi.org/10.1177/0959683610369501

Kumar, N., Kumar, M., Sherring, A., Suryavanshi, S., Ahmad, A. & Lal, D. (2020) Applicability of HEC-RAS 2D and GFMS for flood extent mapping: A case study of Sangam area, Prayagraj, India. *Modeling Earth Systems and Environment*, 6(1), 397–405. Available from: https://doi.org/10.1007/s40808-019-00687-8

Lecce, S.A., Pease, P.P., Gares, P.A. & Rigsby, C.A. (2004) Floodplain sedimentation during an extreme flood: The 1999 flood on the Tar River, eastern North Carolina. *Physical Geography*, 25(4), 334–346. Available from: https://doi.org/10.2747/0272-3646.25.4.334

Leigh, D.S. (2018) Vertical accretion sand proxies of gaged floods along the upper little Tennessee River, blue Ridge Mountains, USA. *Sedimentary Geology*, 364, 342–350. Available from: https://doi.org/10.1016/j.sedgeo.2017.09.007

Liu, Q., Yang, X., Anderson, N.J., Liu, E. & Dong, X. (2012) Diatom ecological response to altered hydrological forcing of a shallow lake on the Yangtze floodplain, SE China. *Ecohydrology*, 5(3), 316–325. Available from: https://doi.org/10.1002/eco.222

McGlue, M.M., Silva, A., Assine, M.L., Stevaux, J.C. & do Pupim, F.N. (2016) Paleolimnology in the pantanal: Using lake sediments to track quaternary environmental change in the world's largest tropical wetland. In: *Handbook of environmental chemistry*. Cham: Springer. Available from: https://doi.org/10.1007/698_2015_350

Munoz, S.E., Giosan, L., Therrell, M.D., Remo, J.W.F., Shen, Z., Sullivan, R. M., et al. (2018) Climatic control of Mississippi River flood hazard amplified by river engineering. *Nature*, 556(7699), 95–98. Available from: https://doi.org/10.1038/nature26145

Munoz, S.E., Gruley, K.E., Massie, A., Fike, D.A., Schroeder, S. & Williams, J.W. (2015) Cahokia's emergence and decline coincided with shifts of flood frequency on the Mississippi River. *Proceedings of the National Academy of Sciences of the United States of America*, 112(20), 6319–6324. Available from: https://doi.org/10.1073/pnas.1501904112

Munoz, S.E., Schroeder, S., Fike, D.A. & Williams, J.W. (2014) A record of sustained prehistoric and historic land use from the cahokia region, Illinois, USA. *Geology*, 42(6), 499–502. Available from: https://doi.org/10.1130/G35541.1

Phillips, J.D. & Slattery, M.C. (2008) Antecedent alluvial morphology and sea-level controls on form-process transition zones in the lower Trinity River, Texas. *River Research and Applications*, 24(3), 293–309. Available from: https://doi.org/10.1002/rra.1060

Phillips, J.D., Slattery, M.C. & Musselman, Z.A. (2004) Dam-to-delta sediment inputs and storage in the lower trinity river, Texas. *Geomorphology*, 62(1-2), 17–34. Available from: https://doi.org/10.1016/j.geomorph.2004.02.004

Phillips, J.D., Slattery, M.C. & Musselman, Z.A. (2005) Channel adjustments of the lower Trinity River, Texas, downstream of Livingston dam. *Earth Surface Processes and Landforms*, 30(11), 1419–1439. Available from: https://doi.org/10.1002/esp.1203

Quirogaa, V.M., Kurea, S., Udoa, K. & Manoa, A. (2016) Application of 2D numerical simulation for the analysis of the February 2014 Bolivian Amazonia flood: Application of the new HEC-RAS version 5. *Ribagua*, 3(1), 25–33. Available from: https://doi.org/10.1016/j.riba.2015.12.001

Reinders, J.B. & Muñoz, S.E. (2021) Improvements to flood frequency analysis on alluvial Rivers using Paleoflood data. *Water Resources Research*, 57(4), e2020WR028631. Available from: https://doi.org/10.1029/2020WR028631

Rowland, J.C., Lepper, K., Dietrich, W.E., Wilson, C.J. & Sheldon, R. (2005) Tie channel sedimentation rates, oxbow formation age and channel migration rate from optically stimulated luminescence (OSL) analysis of floodplain deposits. *Earth Surface Processes and Landforms*, 30(9), 1161–1179. Available from: https://doi.org/10.1002/esp.1268

Shustikova, I., Domeneghetti, A., Neal, J.C., Bates, P. & Castellarin, A. (2019) Comparing 2D capabilities of HEC-RAS and LISFLOOD-FP on complex topography. *Hydrological Sciences Journal*, 64(14), 1769–1782. Available from: https://doi.org/10.1080/02626667.2019.1671982

Smith, V.B. & Mohrig, D. (2017) Geomorphic signature of a dammed Sandy River: The lower Trinity River downstream of Livingston dam in Texas, USA. *Geomorphology*, 297, 122–136. Available from: https://doi.org/10.1016/j.geomorph.2017.09.015

StratMap Lidar Project. (2017) Jefferson, Liberty, & Chambers Counties Lidar. Available from: https://data.tnris.org/collection?c=12342f12-2d74-44c4-9f00-a5c12ac2659c&geo=-94.84595209026342,30.0119509781#9.09/29.8755/-94.3437

Texas Water Development Board. (2022) River Basins. Available from: https://www.twdb.texas.gov/surfacewater/rivers/river_basins/index.asp

Thoms, M.C. (2003) Floodplain-river ecosystems: Lateral connections and the implications of human interference. *Geomorphology*, 56(3-4), 335–349. Available from: https://doi.org/10.1016/S0169-555X(03)00160-0

Toonen, W.H.J. (2015) Flood frequency analysis and discussion of nonstationarity of the lower Rhine flooding regime (AD 1350-2011): Using discharge data, water level measurements, and historical records. *Journal of Hydrology*, 528, 490–502. Available from: https://doi.org/10.1016/j.jhydrol.2015.06.014

Toonen, W.H.J., Kleinhans, M.G. & Cohen, K.M. (2012) Sedimentary architecture of abandoned channel fills. *Earth Surface Processes and Landforms*, 37(4), 459–472. Available from: https://doi.org/10.1002/esp.3189

Toonen, W.H.J., Middelkoop, H., Konijnendijk, T.Y.M., Macklin, M.G. & Cohen, K.M. (2016) The influence of hydroclimatic variability on flood frequency in the lower Rhine. *Earth Surface Processes and Landforms*, 41(9), 1266–1275. Available from: https://doi.org/10.1002/esp.3953

Toonen, W.H.J., Munoz, S.E., Cohen, K.M. & Macklin, M.G. (2020) High-resolution sedimentary Paleoflood Records in Alluvial River Environments: A review of recent methodological advances and application to flood hazard assessment. In: Herget, J. & Fontana, A. (Eds.) *Palaeohydrology. Geography of the physical environment*. Cham: Springer, pp. 213–228. Available from: https://doi.org/10.1007/978-3-030-23315-0_11

Toonen, W.H.J., Winkels, T.G., Cohen, K.M., Prins, M.A. & Middelkoop, H. (2015) Lower Rhine historical flood magnitudes of the last 450years reproduced from grain-size measurements of flood deposits using end member modelling. *Catena*, 130, 69–81. Available from: https://doi.org/10.1016/j.catena.2014.12.004

United States Geological Survey. (2022) USGS Water Data for the Nation. In *National Water Information System:* Web Interface. Available from: https://nwis.waterdata.usgs.gov/tx/nwis/inventory/?site_no=08067000&agency_cd=USGS

USGS Historical Topographic Map Collection. (1984) *Map Liberty Quadrangle 1984*. Available from: https://ngmdb.usgs.gov/topoview/viewer/#12/30.0198/-94.8881

USGS Historical Topographic Map Collection. (1986) *Map Beaumont, Texas 1986*. Available from: https://ngmdb.usgs.gov/topoview/viewer/#12/30.0198/-94.8881

Van Hengstum, P.J., Reinhardt, E.G., Boyce, J.I. & Clark, C. (2007) Changing sedimentation patterns due to historical land-use change in Frenchman's bay, Pickering, Canada: Evidence from high-resolution textural analysis. *Journal of Paleolimnology*, 37(4), 603–618. Available from: https://doi.org/10.1007/s10933-006-9057-y

Vasskog, K., Kvisvik, B.C. & Paasche, Ø. (2016) Effects of hydrogen peroxide treatment on measurements of lake sediment grain-size distribution. *Journal of Paleolimnology*, 56(4), 365–381. Available from: https://doi.org/10.1007/s10933-016-9924-0

Walling, D.E. & Bradley, S.B. (1989) Rates and patterns of contemporary floodplain sedimentation: A case study of the river culm, Devon, UK. *GeoJournal*, 19(1), 53–62. Available from: https://doi.org/10.1007/BF00620549

Wilhelm, B., Ballesteros Cánovas, J.A., Macdonald, N., Toonen, W.H.J., Baker, V., Barriendos, M., et al. (2019) Interpreting historical, botanical, and geological evidence to aid preparations for future floods. *WIREs Water*, 6(1), e1318. Available from: https://doi.org/10.1002/wat2.1318

Yalcin, E. (2020) Assessing the impact of topography and land cover data resolutions on two-dimensional HEC-RAS hydrodynamic model simulations for urban flood hazard analysis. *Natural Hazards*, 101(3), 995–1017. Available from: https://doi.org/10.1007/s11069-020-03906-z

SUPPORTING INFORMATION

Additional supporting information can be found online in the Supporting Information section at the end of this article.

How to cite this article: Reinders, J.B., Sullivan, R.M., Winkler, T.S., van Hengstum, P.J., Beighley, R.E. & Munoz, S.E. (2023) A hydraulic modelling approach to study flood sediment deposition in floodplain lakes. *Earth Surface Processes and Landforms*, 48(4), 756–769. Available from: https://doi.org/10.1002/esp.5515